Electronic Supplementary Information

Role of the Organic Linker in the Early Stages of the Templated Synthesis of Mesoporous Organosilicas

Ryusuke Futamura,[1,†] *José R. B. Gomes,*[1,*] *Miguel Jorge*[2,*]

[1]CICECO, Department of Chemistry, University of Aveiro, Campus Universitário de Santiago, Aveiro 3810-193, Portugal

[2]LSRE - Laboratory of Separation and Reaction Engineering – Associate Laboratory LSRE/LCM, Faculdade de Engenharia, Universidade do Porto, Rua do Dr. Roberto Frias, 4200 - 465 Porto, Portugal

This file contains a description of the computational methods, three tables with the force field parameters used in the molecular dynamics simulations, as well as several additional figures to complement the discussion in the main paper or to support the computational strategy considered.

Computational Methods

Simulations were carried out using the GROMACS 4.5.4 molecular dynamics package.[1,2] The equations of motion were integrated with the Verlet leapfrog algorithm[3] and a time step of 2 fs. The *NpT* ensemble was used for all runs, with the temperature fixed at 298.15 K by applying the Nosé-Hoover thermostat,[4,5] and the pressure fixed at 1 bar by using the Parrinello-Rahman barostat.[6] The simulation boxes were always cubic and periodic in all directions. The total potential energy was calculated as the sum of harmonic angle-bending terms, torsional terms of the Ryckaert-Bellemans form, Lennard-Jones 12-6 terms and Coulomb electrostatic terms. Rigid constraints were enforced on all bond lengths using the LINCS algorithm.[7] Short-range dispersion interactions were handled using a twin-range cutoff scheme, with interactions between the inner and outer radii (1.0 and 1.2 nm respectively) updated every 10 time steps. A long-range dispersion correction term was also added to both energy and pressure. The particle-mesh Ewald method[8] with a real-space cutoff of 1.0 nm was applied to deal with long-range electrostatic interactions.

The SPC/E potential,[9] with rigid bonds and bond angle, was employed to model water molecules. As in previous works, we chose decyltrimethylammonium bromide (DeTAB) as the surfactant,[10,11] which was modeled using a united-atom representation, i.e., all CH_2 and CH_3 groups were represented by a single interaction center. Potential parameters for the head group were taken from Jorgensen and Gao[12] and parameters for the aliphatic tail were taken from Smit et al.[13]. The force-field for the organosilicate species was developed by combining the OPLS-AA potential[14] for the organic moieties with our previous model for anionic silicate species.[10,11] The latter is based on the force field of Pereira et al.[15] for neutral silicates. New values for the bond lengths, angles and point charges of anionic organosilicates were obtained from density

functional theory calculations at the B3LYP/6-311+G(2d,2p) level on a wide range of geometries.[16,17,] A full table of parameters for the organosilicate force field is given in Supporting Information, and more details can be found in previous publications.[11,16,18]

Each of the solutions considered in this work contains 150 $DeTA^+$, 4 Br^- ions and 7500 water molecules, to which were added: i) 71 SIBSI and 4 SIBSN anions to create the solution with benzenesilica; ii) 71 SIEySI and 4 SIEySN anions to create solution with ethylenesilica; iii) 71 SIEaSI and 4 SIEaSN anions to create solution with ethanesilica. The notation SN and SI is used to distinguish neutral $–Si(OH)_3$ and negatively charged (deprotonated) $[–Si(OH)_2O]^-$ fragments, while B, Ey and Ea are used to denote the benzene, ethylene and ethane linkers. Thus, the total number of Si atoms (150) in the three solutions is the same. The relative proportion of SN and SI moieties was also constant and was estimated for a pH of 11[19], corresponding to representative synthesis conditions for organosilica materials.[20] In all cases, the starting configurations for the different solutions were built by randomly dispersing the surfactant, bromide ions and organosilicates in an empty cubic box, and were then solvated with water. To calculate the distribution of surfactant aggregates in each solution, we identified the individual clusters of surfactants present in each sampled configuration using an adaptation of the Hoshen-Kopelman cluster-counting algorithm,[21] with details described elsewhere.[18] To be certain that the results reported here were insensitive to the size of the system and were representative of a pseudo-equilibrium state, we carried out a simulation for the benzenesilicate solution with a system size that was 4 times larger than mentioned above (i.e., over 100000 atoms) for a total of 100 ns. Results obtained in this large run (see Figures S3-S5) were very similar to those of the smaller run, thus validating our approach.

The total potential energy was calculated as the sum of angle-bending terms, torsional terms, dispersion interactions, repulsive interactions and electrostatic interactions. Angles were modeled by a harmonic potential of the form:

$$U = \frac{1}{2} k \left(\theta - \theta_0\right)^2$$

Dihedrals were represented by a Ryckaert-Bellemans (R-B) function, of the form:

$$U = \sum_{n=0}^{5} C_n \left(\cos\left(\varphi\right)\right)^n$$

The intermolecular potential (dispersion, repulsion and electrostatics) is the sum of a Lennard-Jones (L-J) term and a Coulomb term:

$$U_{ij} = 4\varepsilon_{ij}\left[\left(\frac{\sigma_{ij}}{r_{ij}}\right)^{12} - \left(\frac{\sigma_{ij}}{r_{ij}}\right)^{6}\right] + f\frac{q_i q_j}{r_{ij}}$$

In the above equations, U is the potential energy, θ is the instantaneous bond angle, θ_0 is the equilibrium bond angle, k is a harmonic force constant, φ is the instantaneous dihedral angle, C_n are the R-B parameters, σ is the L-J site diameter, ε is the L-J well depth, q is the site partial charge, f is a constant (accounting for the vacuum permittivity) with the value of 138.935485 and r_{ij} is the distance between sites i and j.

Table S1. Lennard-Jones parameters and atomic masses.

Site	σ (nm)	ε (kJ mol^{-1})	Mass (a.u.)	Site	σ (nm)	ε (kJ mol^{-1})	Mass (a.u.)
O_W	0.31656	0.65019	15.9994	**Br**	0.46238	0.37656	79.9040
H_W	0.00000	0.00000	1.0080	**Nh**	0.32500	0.71128	14.0067
$H_{sp}3$	0.25000	0.12552	1.0080	**Ch3**	0.39600	0.60668	15.0345
$H_{sp}2$	0.24200	0.12552	1.0080	**Ch2**	0.39600	0.60668	14.0266
H_A	0.24200	0.12552	1.0080	**Ct3**	0.39300	0.94780	15.0345
$C_{sp}3$(SN)	0.35500	0.27614	12.0110	**Ct2**	0.39300	0.39076	14.0266
$C_{sp}3$(SI)	0.35500	0.27614	12.0110	**Si_N**	0.44350	0.39748	28.0855
$C_{sp}2$(SN)	0.35500	0.31798	12.0110	**Oh_N**	0.34618	0.66567	15.9994
$C_{sp}2$(SI)	0.35500	0.31798	12.0110	**Ho_N**	0.23541	0.41338	1.0080
C_A(SN)	0.35500	0.29288	12.0110	**Si_I**	0.44350	0.39748	28.0855
C_A(SI)	0.35500	0.29288	12.0110	**Oh_I**	0.34618	0.66567	15.9994
C_A(H)	0.35500	0.29288	12.0110	**Ho_I**	0.23541	0.41338	1.0080
				Oc	0.34618	0.66567	15.9994

Atom types are denoted as follows: The water molecule consists of three sites, one oxygen (O_W) and two hydrogens (H_W). The bromide ion is modeled by a single site (Br). The united-atom $DeTA^+$ surfactant molecule consists of one head-nitrogen atom (Nh), three head-CH_3 sites (Ch3), one head-CH_2 site (Ch2), 8 tail-CH_2 sites (Ct2) and one tail-CH_3 site (Ct3). The neutral $–Si(OH)_3$ fragment consists of one silicon atom (Si_N), three hydroxyl oxygens (Oh_N) and three hydroxyl hydrogens (Ho_N). The negatively charged $[–Si(OH)_2O]^-$ fragment consists of one silicon atom (Si_I), two hydroxyl oxygens (Oh_I), two hydroxyl hydrogens (Ho_I) and one anionic oxygen (Oc). The benzene linker consists of six carbon (C_A) and 4 hydrogen (H_A) atoms. The ethylene linker consists of two carbon ($C_{sp}2$) and two hydrogen ($H_{sp}2$) atoms. The ethane linker consists of two carbon ($C_{sp}3$) and four hydrogen ($H_{sp}3$) atoms. In the case of the organic linkers, SN, SI and H in parentheses are used to denote atoms directly bonded to a neutral silicate, to an anionic silicate or to a hydrogen atom, respectively.

Table S2. Geometric parameters and point charges for neutral and anionic organosilicates together with harmonic force constants.

atom	charge (a.u.)	bond	length (nm)	angle	θ_0 (°)	k (kJ mol^{-1} rad^{-2})
Si_N	1.206	Si_N-O	0.165	Si_N-Oh_N-Ho_N	114.4	103.460
Si_I	1.332	Si_I-O	0.169	Si_I-Oh_I-Ho_I	109.8	103.460
Oh_N	-0.762	Si_I-O_c	0.158	Oh_N-Si_N-Oh_N	109.6	232.960
Oh_I	-0.839	Oh-Ho	0.097	Oh_I-Si_I-Oh_I	104.9	232.960
Oc	-1.046	Si_N-C	0.186	Oh_I-Si_I-O_c	114.2	232.960
Ho_N	0.405	Si_I-C	0.190	Oh_N-Si_N-C	111.0	412.620
Ho_I	0.376	$C_{sp}3$-$C_{sp}3$	0.153	Oh_I-Si_I-C	103.7	412.620
$H_{sp}3$	0.060	$C_{sp}3$-$H_{sp}3$	0.109	O_c-Si_I-C	116.4	412.620
$H_{sp}2$	0.115	$C_{sp}2$-$C_{sp}2$	0.134	Si-$C_{sp}3$-$C_{sp}3$	115.4	488.273
H_A	0.115	$C_{sp}2$-$H_{sp}2$	0.108	Si-$C_{sp}2$-$C_{sp}2$	126.0	585.760
$C_{sp}3$(SN)	-0.255	C_A-C_A	0.140	Si-C_A-C_A	120.0	292.880
$C_{sp}3$(SI)	-0.480	C_A-H_A	0.108	Si-$C_{sp}3$-$H_{sp}3$	109.9	313.800
$C_{sp}2$(SN)	-0.250			Si-$C_{sp}2$-$H_{sp}2$	117.6	292.880
$C_{sp}2$(SI)	-0.475			$C_{sp}3$-$C_{sp}3$-$H_{sp}3$	110.7	313.800
C_A(SN)	-0.135			$H_{sp}3$-$C_{sp}3$-$H_{sp}3$	107.8	276.144
C_A(SI)	-0.360			$C_{sp}2$-$C_{sp}2$-$H_{sp}2$	120.0	292.880
C_A(H)	-0.115			C_A-C_A-C_A	120.0	527.184
				C_A-C_A-H_A	120.0	292.880

Atom types are denoted as follows: Si is a silicon atom, Oh is a hydroxyl oxygen atom, Oc is a deprotonated oxygen atom (negative charge), Ho is a hydroxyl hydrogen atom, H is a hydrogen atom in an organic group, and C is a carbon atom. For the latter two atom types, subscript A refers to a phenyl group, subscript sp2 refers to an ethylene group and subscript sp3 refers to an ethane group. Furthermore, subscripts N and I are used to denote whether atom types belong to a neutral or to an anionic fragment, respectively. Finally, the notation SN and SI is used to distinguish neutral $-Si(OH)_3$ and negatively charged (deprotonated) $[-Si(OH)_2O]^-$ fragments, i.e., for instance, C_A(SN) and C_A(SI) are used to label the carbon atoms in the benzyl ring of benzenesilica that are bonded directly to the neutral $-Si(OH)_3$ or to the negatively charged $[-Si(OH)_2O]^-$ fragments, respectively.

Table S3. Dihedral potential parameters for the surfactant and for the organosilicates.

Dihedral	C_0 (kJ mol^{-1})	C_1 (kJ mol^{-1})	C_2 (kJ mol^{-1})	C_3 (kJ mol^{-1})	C_4 (kJ mol^{-1})	C_5 (kJ mol^{-1})
Ch – Nh – Ch – Ct	3.0418	-1.3514	0.5188	-2.2092	0.0	0.0
Nh – Ch – Ct – Ct	8.3973	16.7862	1.1339	-26.3174	0.0	0.0
Ch – Ct – Ct – Ct	8.3973	16.7862	1.1339	-26.3174	0.0	0.0
Ct – Ct – Ct – Ct	8.3973	16.7862	1.1339	-26.3174	0.0	0.0
Oh_N – Si_N – Oh_N – Ho_N	14.8473	9.1554	-3.6233	2.0686	0.0	0.0
Oh_I – Si_I – Oh_I – Ho_I	14.8473	9.1554	-3.6233	2.0686	0.0	0.0
Oc – Si_I – Oh_I – Ho_I	14.8473	9.1554	-3.6233	2.0686	0.0	0.0
C_A – Si_N – Oh_N – Ho_N	15.2038	23.8622	-2.5673	-9.8910	0.00000	0.00000
C_A – Si_I – Oh_I – Ho_I	15.2038	23.8622	-2.5673	-9.8910	0.00000	0.00000
$C_{sp}3$ – Si_N – Oh_N – Ho_N	15.2038	23.8622	-2.5673	-9.8910	0.00000	0.00000
$C_{sp}3$ – Si_I – Oh_I – Ho_I	15.2038	23.8622	-2.5673	-9.8910	0.00000	0.00000
$C_{sp}2$ – Si_N – Oh_N – Ho_N	15.2038	23.8622	-2.5673	-9.8910	0.00000	0.00000
$C_{sp}2$ – Si_I – Oh_I – Ho_I	15.2038	23.8622	-2.5673	-9.8910	0.00000	0.00000
C_A – C_A – Si_N – Oh_N	0.00000	0.00000	0.00000	0.00000	0.00000	0.00000
C_A – C_A – Si_I – Oh_I	0.00000	0.00000	0.00000	0.00000	0.00000	0.00000
C_A – C_A – Si_I – Oc	0.00000	0.00000	0.00000	0.00000	0.00000	0.00000
$C_{sp}3$ – $C_{sp}3$ – Si_N – Oh_N	0.34987	1.04960	0.00000	-1.39946	0.00000	0.00000
$C_{sp}3$ – $C_{sp}3$ – Si_I – Oh_I	0.34987	1.04960	0.00000	-1.39946	0.00000	0.00000
$C_{sp}3$ – $C_{sp}3$ – Si_I – Oc	0.34987	1.04960	0.00000	-1.39946	0.00000	0.00000
$C_{sp}2$ – $C_{sp}2$ – Si_N – Oh_N	0.00000	0.00000	0.00000	0.00000	0.00000	0.00000
$C_{sp}2$ – $C_{sp}2$ – Si_I – Oh_I	0.00000	0.00000	0.00000	0.00000	0.00000	0.00000
$C_{sp}2$ – $C_{sp}2$ – Si_I – Oc	0.00000	0.00000	0.00000	0.00000	0.00000	0.00000

(continues next page)

Table S3. (cont.)

Dihedral	C_0 (kJ mol^{-1})	C_1 (kJ mol^{-1})	C_2 (kJ mol^{-1})	C_3 (kJ mol^{-1})	C_4 (kJ mol^{-1})	C_5 (kJ mol^{-1})
$H_{sp}3 - C_{sp}3 - Si_N - Oh_N$	0.41900	1.25700	0.00000	-1.67600	0.00000	0.00000
$H_{sp}3 - C_{sp}3 - Si_I - Oh_I$	0.41900	1.25700	0.00000	-1.67600	0.00000	0.00000
$H_{sp}3 - C_{sp}3 - Si_I - Oc$	0.41900	1.25700	0.00000	-1.67600	0.00000	0.00000
$H_{sp}2 - C_{sp}2 - Si_N - Oh_N$	1.50212	4.50635	0.00000	-6.00846	0.00000	0.00000
$H_{sp}2 - C_{sp}2 - Si_I - Oh_I$	1.50212	4.50635	0.00000	-6.00846	0.00000	0.00000
$H_{sp}2 - C_{sp}2 - Si_I - Oc$	1.50212	4.50635	0.00000	-6.00846	0.00000	0.00000
$H_A - C_A - C_A - Si_N$	30.33400	0.00000	-30.33400	0.00000	0.00000	0.00000
$H_A - C_A - C_A - Si_I$	30.33400	0.00000	-30.33400	0.00000	0.00000	0.00000
$C_A - C_A - C_A - Si_N$	30.33400	0.00000	-30.33400	0.00000	0.00000	0.00000
$C_A - C_A - C_A - Si_I$	30.33400	0.00000	-30.33400	0.00000	0.00000	0.00000
$Si_N - C_{sp}3 - C_{sp}3 - Si_N$	2.92880	-1.46440	0.20920	-1.67360	0.00000	0.00000
$Si_N - C_{sp}3 - C_{sp}3 - Si_I$	2.92880	-1.46440	0.20920	-1.67360	0.00000	0.00000
$Si_I - C_{sp}3 - C_{sp}3 - Si_I$	2.92880	-1.46440	0.20920	-1.67360	0.00000	0.00000
$Si_N - C_{sp}2 - C_{sp}2 - Si_N$	58.57600	0.00000	-58.57600	0.00000	0.00000	0.00000
$Si_N - C_{sp}2 - C_{sp}2 - Si_I$	58.57600	0.00000	-58.57600	0.00000	0.00000	0.00000
$Si_I - C_{sp}2 - C_{sp}2 - Si_I$	58.57600	0.00000	-58.57600	0.00000	0.00000	0.00000
$Si_N - C_{sp}3 - C_{sp}3 - H_{sp}3$	0.62760	1.88280	0.00000	-2.51040	0.00000	0.00000
$Si_I - C_{sp}3 - C_{sp}3 - H_{sp}3$	0.62760	1.88280	0.00000	-2.51040	0.00000	0.00000
$Si_N - C_{sp}2 - C_{sp}2 - H_{sp}2$	58.57600	0.00000	-58.57600	0.00000	0.00000	0.00000
$Si_I - C_{sp}2 - C_{sp}2 - H_{sp}2$	58.57600	0.00000	-58.57600	0.00000	0.00000	0.00000

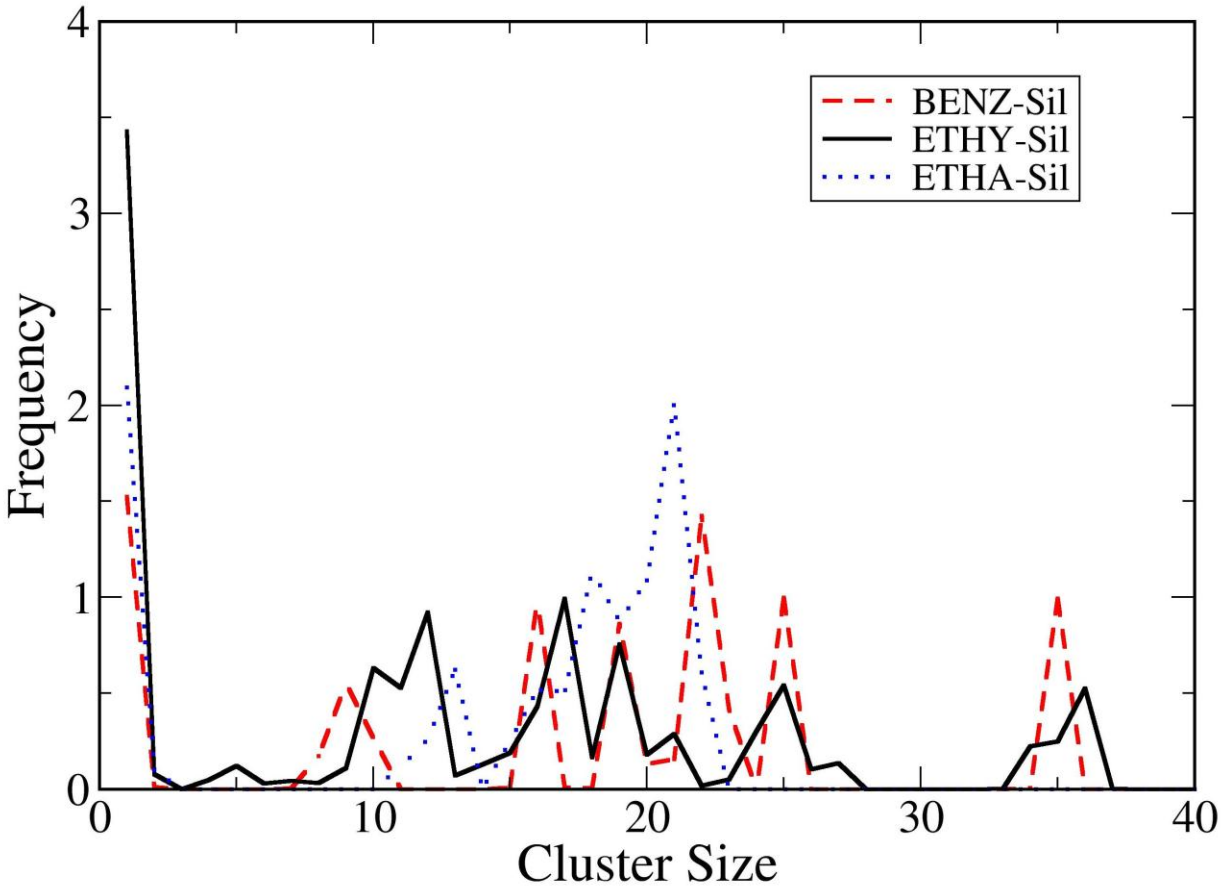

Figure S1. Comparison of the cluster size distributions (CSDs) obtained in the solutions with benzenesilica (red dashed line), ethylenesilica (black solid line), and ethanesilica (blue dotted line). The CSDs for benzenesilica and ethylenesilica are similar, while the one for ethanesilica shows no micelles above a size of ~22 surfactants.

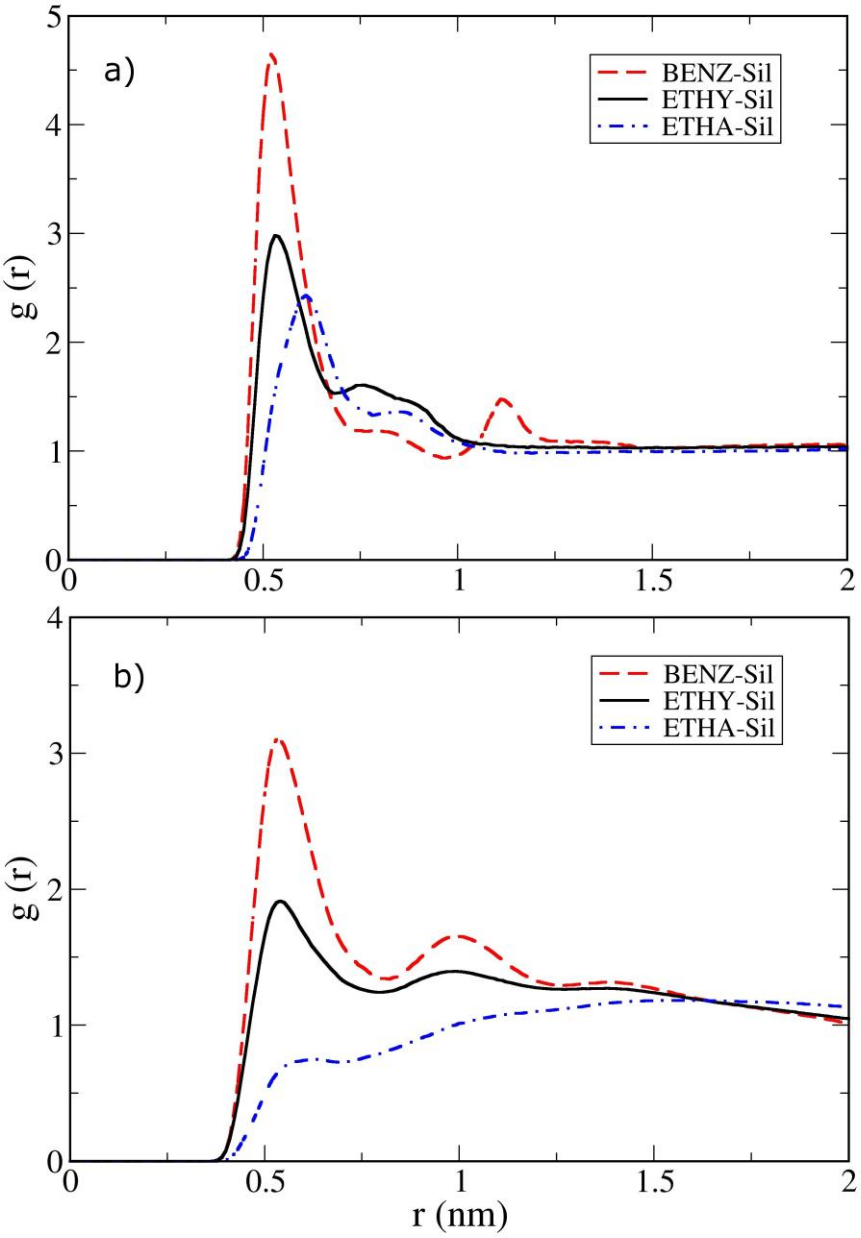

Figure S2. Selected radial distribution functions obtained in the solutions with benzenesilica (red dashed line), ethylenesilica (black solid line), and ethanesilica (blue dotted line) for the interactions between: a) Si atoms and N atoms of the surfactant heads; b) Si atoms and surfactant tail atoms. In the first case, the peaks for benzenesilica and ethylenesilica are located at the same position, while the peak for ethanesilica is broader and shifted to the right. In the second case, the differences are even more evident, showing very little interaction of ethanesilica with the surfactant tails. These results confirm that benzenesilica and ethylenesilica are predominantly oriented parallel to the micelle surface, while ethanesilica is much more disordered, with a preferentially perpendicular orientation.

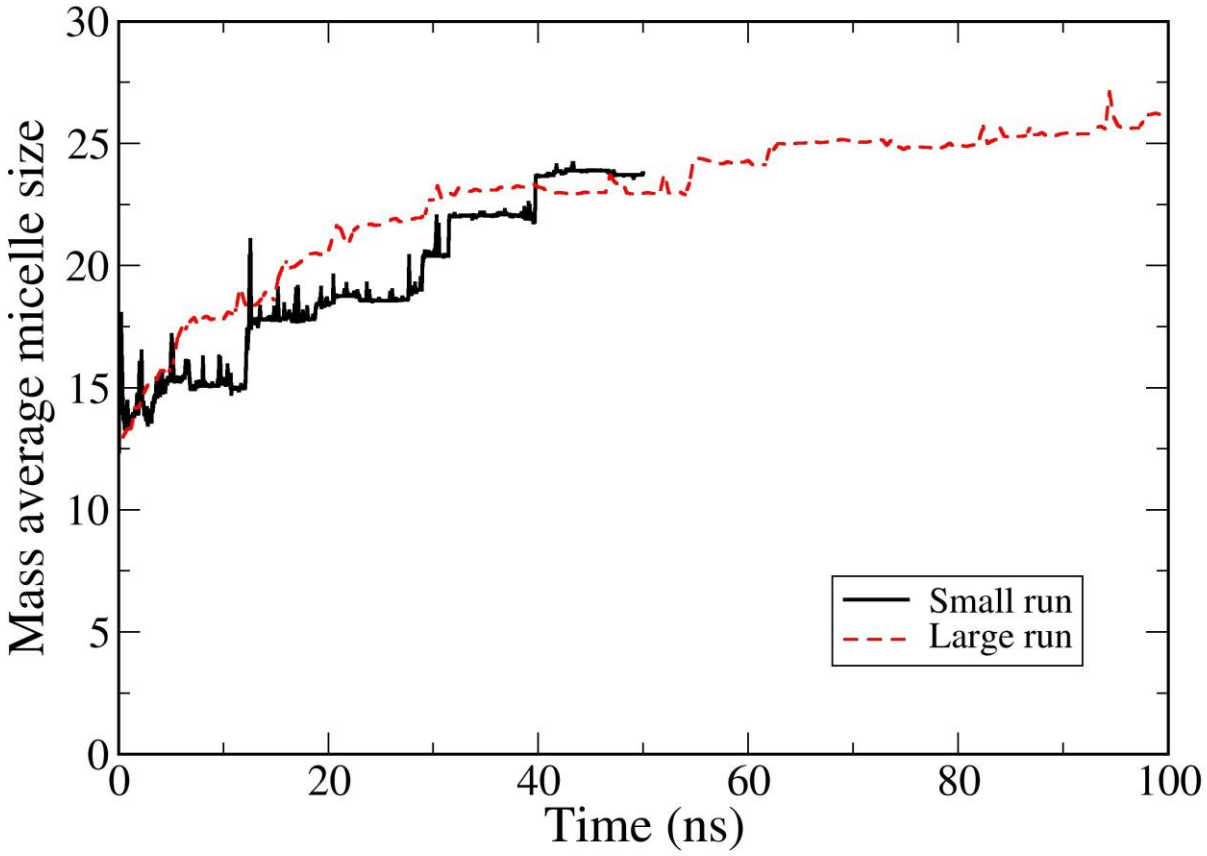

Figure S3. Mass-average micelle size as a function of simulation time for two independent runs of the solution with benzenesilica. The "small run" corresponds to the results shown in the main paper, while the "large run" was carried out for twice as long in a system 4 times as large. There is only a small increase from (23 to 25) in the mass average micelle size for the large run, suggesting that both systems reached a pseudo-equilibrium state.

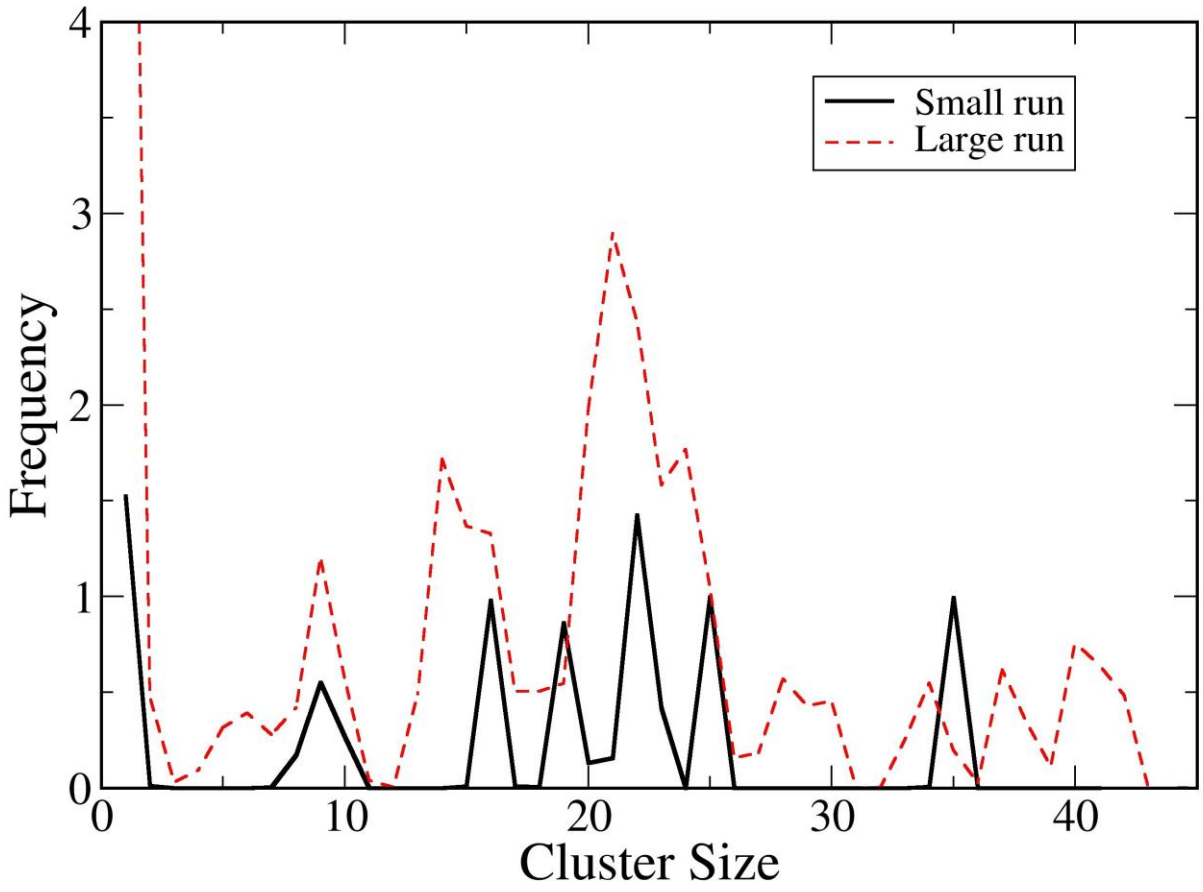

Figure S4. Cluster size distribution for two independent runs of the solution with benzenesilica, as described in the caption of Figure S3. Both distributions span approximately the same range of micelle sizes, and in both cases the most predominant population is for micelles around 20-25 surfactants.

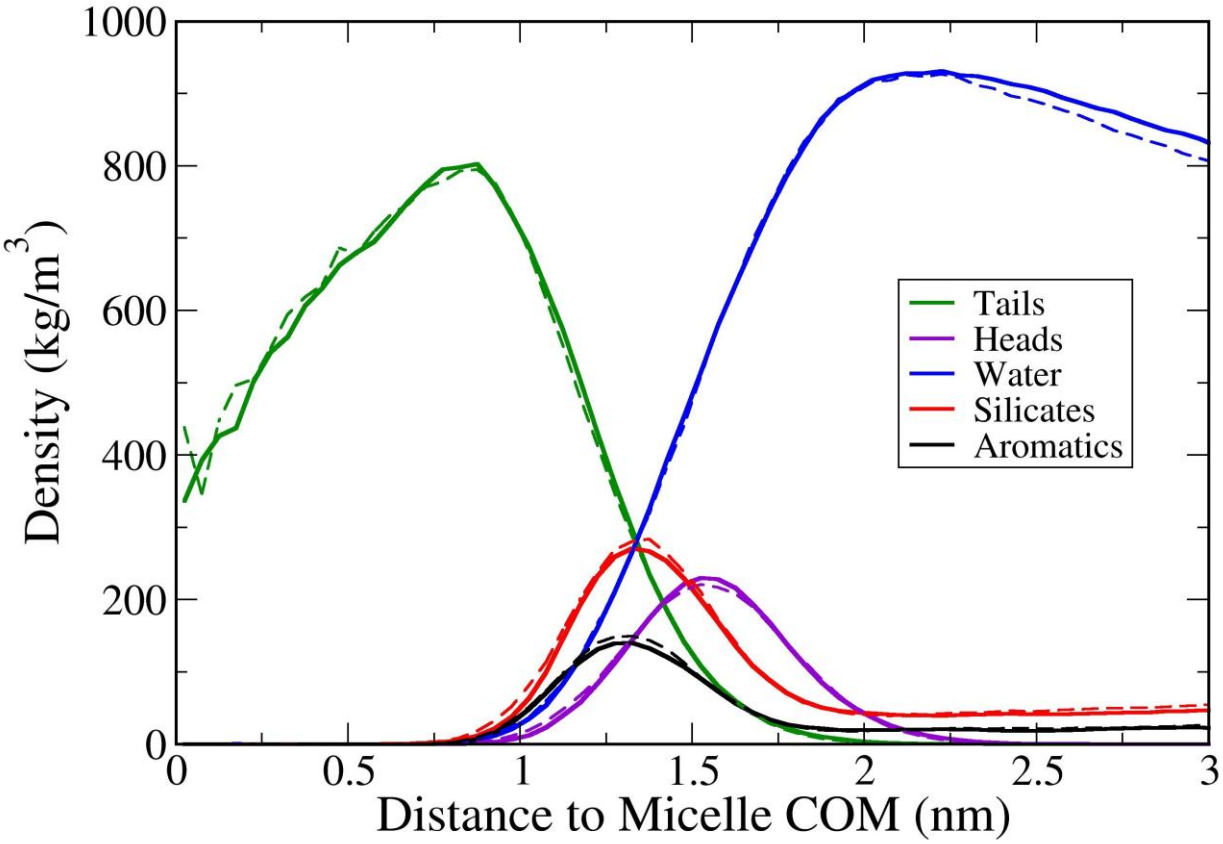

Figure S5. Radial density profiles for micelles of ~35 surfactants obtained in two independent runs of the solution with benzenesilica, as described in the caption of Figure S3. Both sets of profiles are virtually indistinguishable, showing that the results presented in the paper are not dependent on system size.

References

1 van der Spoel, D.; Lindahl, E.; Hess, B.; van Buuren, A. R.; Apol, E.; Meulenhoff, P. J.; Tieleman, D. P.; Sijbers, A. L. T. M.; Feenstra, K. A.; van Drunen, R.; Berendsen, H. J. C. Gromacs User Manual version 4.5.4, www.gromacs.org, 2010.

2 Berendsen, H. J. C.; van der Spoel, D.; van Drunen, R. GROMACS: A Message-Passing Parallel Molecular Dynamics Implementation. *Comp. Phys. Comm.* **1995**, *91*, 43-56.

3 Hockney, R. W.; Goel, S. P.; Eastwood, J. W. Quiet high-resolution computer models of a plasma. *J. Comput. Phys.* **1974**, *14*, 148-158.

4 Nosé, S. A Molecular Dynamics Method for Simulations in the Canonical Ensemble. *Mol. Phys.* **1984**, *52*, 255-268.

5 Hoover, W. G. Canonical Dynamics: Equilibrium Phase-Space Distributions. *Phys. Rev. A* **1985**, *31*, 1695-1697.

6 Parrinello, M.; Rahman, A. Polymorphic Transitions in Single Crystals: A New Molecular Dynamics Method. *J. Appl. Phys.* **1981**, *52*, 7182-7190.

7 Hess, B.; Bekker, H.; Berendsen, H. J. C.; Fraaije, J. G. E. M. LINCS: A Linear Constraint Solver for Molecular Simulations. *J. Comp. Chem.* **1997**, *18*, 1463-1472.

8 Essman, U.; Perela, L.; Berkowitz, M. L.; Darden, T.; Lee, H.; Pedersen, L. G. A Smooth Particle Mesh Ewald Method. *J. Chem. Phys.* **1995**, *103*, 8577-8593.

9 Berendsen, H. J. C.; Grigera, J. R.; Straatsma, T. P. The Missing Term in Effective Pair Potentials. *J. Phys. Chem.* **1997**, *91*, 6269-6271.

10 Jorge, M.; Gomes, J. R. B.; Cordeiro, M. N. D. S.; Seaton, N. A. Molecular Simulation of Silica/Surfactant Self-Assembly in the Synthesis of Periodic Mesoporous Silicas. *J. Am. Chem. Soc.* **2007**, *129*, 15414-15415.

11 Jorge, M.; Gomes, J. R. B.; Cordeiro, M. N. D. S.; Seaton, N. A. Molecular Dynamics Simulation of the Early Stages of the Synthesis of Periodic Mesoporous Silica. *J Phys Chem. B* **2009**, *113*, 708-718.

12 Jorgensen, W. L.; Gao, J. Monte Carlo simulations of the hydration of ammonium and carboxylate ions. *J. Phys. Chem.* **1986**, *90*, 2174-2182.

13 Smit, B.; Karaborni, S.; Siepmann, J. I. Computer Simulation of Vapor-Liquid Phase Equilibria of n-Alkanes. *J. Chem. Phys.* **1995**, *102*, 2126-2140.

14 Jorgensen, W.L.; Tirado-Rives, J. The OPLS [optimized potentials for liquid simulations] potential functions for proteins, energy minimizations for crystals of cyclic peptides and crambin. *J. Am. Chem. Soc.* **1988**, *110*, 1657-1666.

15 Pereira, J. C. G.; Catlow, C. R. A.; Price, G. D. Molecular Dynamics Simulation of Methanolic and Ethanolic Silica-Based Sol−Gel Solutions at Ambient Temperature and Pressure. *J. Phys. Chem. A* **2002**, *106*, 130-148.

16 Futamura, R.; Jorge, M.; Gomes, J. R. B. Structures and Energetics of Organosilanes in the Gaseous Phase: A Computational Study. *Theor. Chem. Acc.* **2013**, *132*, 1323-1:10.

17 Gomes, J. R. B.; Cordeiro, M. N. D. S.; Jorge M. Gas-Phase Molecular Structure and Energetics of Anionic Silicates. *Geochim. Cosmochim. Acta.* **2008**, *72*, 4421-4439.

18 Jorge, M. Molecular Dynamics Simulation of Self-Assembly of n-Decyltrimethylammonium Bromide Micelles. *Langmuir* **2008**, *24*, 5714-5725.

19 Šefčík, J.; McCormick, A. V. Thermochemistry of Aqueous Silicate Solution Precursors to Ceramics. *AIChE J.* **1997**, *43*, 2773-2784.

20 Inagaki, S.; Guan, S.; Ohsuna, T.; Terasaki, O. An Ordered Mesoporous Organosilica Hybrid Material with a Crystal-Like Wall Structure. *Nature* **2002**, *416*,304-307.

21 Hoshen, J.; Kopelman, R. Percolation and Cluster Distribution. I. Cluster Multiple Labeling Technique and Critical Concentration Algorithm. *Phys. Rev. B* **1976**, *14*, 3438-3445.